Progress In Electromagnetics Research, PIER 81, 197–212, 2008

NUMERICAL SIMULATION OF THE PROPAGATION OF EM PULSE THROUGH LOSSLESS NON-UNIFORM DIELECTRIC SLAB USING CHARACTERISTIC-BASED METHOD

M. Ho, F.-S. Lai, S.-W. Tan, P.-W. Chen

Department of Electronic Engineering
WuFeng Institute of Technology
Taiwan 621, R. O. C.

Abstract—This paper demonstrates the one-dimensional computational results of the propagation of Gaussian electromagnetic pulse through dielectric slabs of finite thickness with variation in permittivity. The numerical approach used is the characteristic-based method solving the time-domain Maxwell curl equations involved with non-uniform permittivity. In the numerical model, all dielectric slabs are assumed to be isotropic, lossless, and linear. The permittivity of dielectric slab may increase or decrease linearly or sinusoidally. The numerical permittivity is finely discretized such that the variation between two adjacent grids is so small that the non-uniform permittivity is assumed to be piecewise continuous and consequently can be modeled as an individual block. The numerical results of various electric fields, both in the time- and frequency-domain, are presented and compared based on the dielectric slab of constant permittivity for close investigating the effects of the non-uniform permittivity distribution on the electromagnetic fields. It is also shown that under certain arrangement of Gaussian electromagnetic pulse and dielectric slab thickness the pattern of field propagation, reflection and transmission, can be reproduced in different time scales and frequency ranges.

1. INTRODUCTION

The main purpose of this paper is to numerically demonstrate the propagation of electromagnetic pulse through dielectric slabs featured with non-uniform permittivity distribution and hence to observe the effects of such dielectric slabs on the electromagnetic fields. The numerical solutions were obtained through the application of

the characteristic-based method to the time-domain Maxwell curl equations associated with medium whose dielectric constant is non-uniformly distributed in either linear or sinusoidal form. Numerical method sometimes can simulate problems that are nonlinear or involve something complicated, and especially whose analytical solutions are most unlikely available. Complex medium may grant a stage that numerical simulation can play an important role and hopefully provide computational results that might be a torch in the dark area for researchers and engineers. These goals can be realized through the computational reflected and transmitted electric fields, and those inside the dielectrics. The corresponding spectra can provide useful information in the frequency domain. Since the dielectric constant of medium is not uniformly distributed, the analytical solution of such nonlinear problems can not be trivial. The attempt to understand and predict the electromagnetic characteristics for these types of medium then strongly depends upon accurate numerical methods. Thanks to the dramatic advances in computing engineering and the development of numerical algorithms, the heavy demands on memory storage, speed, and scheme accuracy for computation are satisfactory to certain level for detailed numerical modeling.

For the past several decades, metamaterial and composite medium have been drawing significant attentions from many researchers in a variety of applications for the reasons that they display quite different electromagnetic characteristics from their original components. Topics on the theoretical analysis, device design, and fabrication of metamaterials can be easily found [1–5]. Studies of rain medium for analytical expression of equivalent permittivity [6] and as random statistically isotropy mixture [7] were carried out. Reports on the left-handed dielectric materials [8–13] in conjunction with microstrip antennas, directional waveguides and other possible applications are also published. Though the area of complex media, artificial materials or meta-materials have been of great interest, to design and to manufacture one is a rather complicated, sophisticated, and time-consuming task requiring strong theoretical background and engineering supports. In the meantime, many numerical simulation techniques are developed and widely applied to a variety of engineering problems providing useful information and physical trends for designers and engineers. Computational scheme most of time serves as a predictor and/or corrector prior to turning blueprint into molding.

In the recent half century various computational techniques have been applied to many areas such as fluid dynamics, mechanics, electromagnetics, and etc. For the electromagnetic related problems they numerically solve Maxwell's equations in either the frequency

domain or the time domain. Among a variety of approaches, the two most widely used numerical methods have been the method of moment (MoM) and finite-difference time-domain (FDTD) technique since they were proposed in the 1960s. The characteristic-based method was recently developed for numerical approximation of the time-dependent Maxwell's curl equations. In the early 1990s, Whitfield and Janus applied the characteristic-based method to the solutions of fluid dynamic problems [14]. Shang employed it to solve the time-domain Maxwell's equations [15] through an application of explicit central-difference scheme for spatial and temporal derivatives. Its implicit formulation was developed for the same purpose and its results were found to agree with data produced by FDTD [16]. It is also shown that the characteristic-based method can predict the reflection of electromagnetic fields from moving/vibrating perfect conductor in one dimension [17, 18], the effects of finite conductivity on the reflection/transmission of electromagnetic fields [19], and the reflection/transmission of electromagnetic field propagation onto moving dielectric half space [20]. Unlike MoM and FDTD where all field components are placed at the grid nodes, the characteristic-based method defines all field quantities in the center of the grid cell. It directly approximates the time-dependent Maxwell curl equations in the curvilinear system by evaluating the flux across every cell face and then balancing them within each computational cell.

2. GOVERNING EQUATIONS AND MODEL OF DIELECTRIC SLAB

For problems involving with the propagation of electromagnetic fields inside dielectric material are generally described by the time-dependent Maxwell's equations:

$$\frac{\partial \vec{B}}{\partial t} + \nabla \times \vec{E} = 0 \tag{1}$$

$$\frac{\partial \vec{D}}{\partial t} - \nabla \times \vec{H} = 0 \tag{2}$$

$$\nabla \cdot \vec{D} = 0 \tag{3}$$

$$\nabla \cdot \vec{B} = 0. \tag{4}$$

where $\vec{E}$ and $\vec{H}$ are the electric and magnetic field intensities, $\vec{D}$ and $\vec{B}$ are the electric and magnetic flux densities, respectively. These field

components are related through the constitution equations:

$$\vec{D} = \varepsilon_o \varepsilon_r \vec{E} \tag{5}$$

$$\vec{B} = \mu_o \mu_r \vec{H} \tag{6}$$

where ε_o and μ_o are the permittivity and permeability of vacuum, ε_r and μ_r are the dielectric constant and relative permeability of medium, respectively. For non-magnetic materials as in this study the relative permeability μ_r is equal to unity.

For the numerical formulation, we need a two-dimensional formulation for the present simulation since the fields are transverse. The Maxwell curl equations, after cast in the Euler equation form and transformed from the Cartesian coordinate system (t, x, y) into a curvilinear coordinate system (τ, ξ, η), can be rewritten as

$$\frac{\partial Q}{\partial \tau} + \frac{\partial F}{\partial \xi} + \frac{\partial G}{\partial \eta} = 0 \tag{7}$$

where $Q = Jq$, $F = J(\xi_x f + \xi_y g)$, $G = J(\eta_x f + \eta_y g)$, and $J = |\frac{\partial x}{\partial \xi}\frac{\partial y}{\partial \eta} - \frac{\partial x}{\partial \eta}\frac{\partial y}{\partial \xi}|$. The symbol J stands for the Jacobian of the inverse transformation, and other three variable vectors are $q = [0,\ B_y,\ D_z]^T$, $f = [0,\ -E_z,\ -H_y]^T$, $g = [E_z,\ 0,\ H_x]^T$, respectively. It is noted that the H_x and B_x are zero in magnitude since the incident electromagnetic fields are set to propagate in the x-direction in the numerical model. By applying the central difference operator

$$\delta_k(\varphi) = (\varphi)_{k+1/2} - (\varphi)_{k-1/2} \tag{8}$$

to (7), we have

$$\frac{Q^{n+1} - Q^n}{\Delta \tau} + \frac{\delta_i F}{\Delta \xi} + \frac{\delta_j G}{\Delta \eta} = 0. \tag{9}$$

In the definition of the central difference operator the subscript (k) indicates the kth computational cell and the field quantity is evaluated at the center of the grid, the two half-integer indices represent the two interfaces either side of the cell of interest at which the corresponding fluxes are evaluated, the symbol φ can be either variable vector F or G. The superscripts (n) and $(n+1)$ on the variable vector Q in (9) are two consecutive time levels. The temporal differentiation in Q, $(Q^{n+1} - Q^n)$, is the flux changes that the proposed method solves for. Accordingly, the numerical method approximates the Maxwell's curl equation in curvilinear coordinate system by solving the flux changes within each grid cell in the time domain.

For the present simulation, we are also interested in observing how the non-uniform permittivity affects the electromagnetic fields. In order to have better presentation of the variation in permittivity we use a fine spatial discretization at the cost of significant increase in computational storage and CPU time. In order to have close examination on the computational results, a uniform dielectric slab (constant ε_r) is used to serve as a basis of comparison and the non-uniform relative permittivity, $\varepsilon_r(x)$, a position dependent variable, is allowed to vary in different ways about one specified value of $\varepsilon_r = 4$. This is illustrated in Figure 1 where only three cases are depicted, one uniform and two non-uniform permittivity distributions. As shown, one increases sinusoidally from $(\varepsilon_r - \Delta)$ to $(\varepsilon_r + \Delta)$ and the other decreases linearly from $(\varepsilon_r + \Delta)$ to $(\varepsilon_r - \Delta)$. Note that they all have identical mean value ε_r. When the dielectric slab is numerically modeled, and since the characteristic-based method places all field components in the grid center, the varying dielectric constant $\varepsilon_r(x)$ at each cell face is well defined while that in the cell center is approximated as the averaged value of the two cell faces.

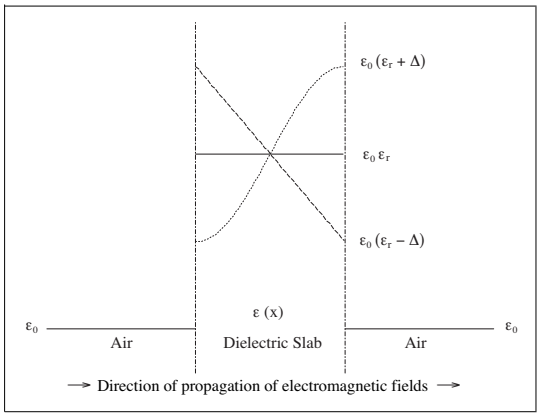

Figure 1. Permittivity as function of position, $\varepsilon_r(x)$. (Solid: uniform, dotted: increases sinusoidally, dashed: decreases linearly).

Due to the nature of the present numerical method, the application of boundary conditions is quite straightforward. There are two types of boundary conditions used in the present simulation. At the air-medium or medium-air interface the proper boundary conditions ensure that both the tangential components of total field intensities are continuous. At the outer layer where the computational domain is truncated the boundary conditions are to guarantee that there exists no reflection of electromagnetic fields from these surfaces. Since the computational

domain is chosen so that the entire numerical incident electromagnetic pulse is initially located inside the domain and starts to propagate toward the dielectric slab, the outer boundary conditions are simply set to be transparent to the outward propagating fields.

3. CASES STUDIED

The incident electromagnetic pulse employed in the present simulation has the following properties. The maximum value of the electric field intensity of the incident pulse is set to be 1 V/m. The electromagnetic pulse is plane and truncated by a rectangular window at 100 dB level with respect to the peak value, in Gaussian distribution form, and can have one of the following pulse widths (in the unit of picoseconds): 694.6578, 15.2825, 6.9466, and 0.2084. The highest frequency contents in the corresponding spectra are about 1.1, 50, 109.9, and 3664.8 GHz, respectively. The thicknesses of slabs are 50 cm, 11 mm, 5 mm, and 150 μm, respectively. The dielectric slabs are isotropic, lossless, linear, made of non-magnetic material ($\mu_r = 1$), have the same mean dielectric constant value of 4 ($\varepsilon_r = 4$) and hence refractive index of 2. Electromagnetic pulse then propagates inside the uniform slab with a velocity of 0.5 c_o where c_o stands for the speed of light and equals exactly 3×10^8 m/s in the numerical model. The reference slab has a uniform permittivity of 4, while the dielectric constant of non-uniform slabs can vary in either sinusoidal or linear type with a maximum dielectric constant deviation Δ being either 0.5 ($3.5 \leq \varepsilon_r \leq 4.5$) or 1.0 ($3.0 \leq \varepsilon_r \leq 5.0$).

In order to capture the transient behavior of the electromagnetic fields, three sampling points are positioned as below. The reflected fields are sampled at 1.05 m, 10.5 mm, 23.1 mm, and 315 μm in front of the slab; the transmitted fields are recorded at 1 m, 10 mm, 22 mm, and 300 μm behind the slab; and the fields inside the medium are observed at the middle point of the slab. Both the time-domain computational results and their spectra are demonstrated in a side-by-side fashion for close observations. The frequency-domain results are obtained through the Fourier transformation of the time-domain data.

Since all dielectric slabs have identical mean permittivity value, it is then expected to observe the following phenomena. The transmitted fields through any two complementary dielectric slabs should bear alike characteristics because the fields experience similar but reciprocal processes. Fields inside different slabs should reveal the type of permittivity distribution for the fact that the fields propagate slower in denser medium and faster in looser medium. Similarly, the strength of the reflected fields reveal what type of dielectric slab from which

they have been bounced from and gone through when compared to the known information.

In order to minimize the discretization error, the grid density is set to be 500 cells per slab at the expense of computing efforts. For the case where the maximum dielectric constant deviation $\Delta = 1.0$ and the variation type is sinusoidal, the minimum and maximum differences between two adjacent cells are 0.0015% and 0.1571% with respect to the mean value. And it is consistent 0.1% for linear case. Though these differentiations are grid density dependent, it is not in the scope of the present study to discuss such problem.

4. RESULTS

We begin this section by introducing a couple of results from observations on the computational data. In the present study there are four sets of model simulated: four electromagnetic pulses of various pulse widths as excitation sources propagate onto four sets of dielectric slabs having different thicknesses with either uniform or non-uniform permittivity distribution. Under particular arrangement of the pulse width and slab thickness, it is found that four sets of various fields reveal identical behavior except in different time or frequency scales. Therefore we will demonstrate computational results in an alternative way, since they display identical trends except the time scales or frequency ranges.

Illustrated in Figure 2 are five electric fields inside different

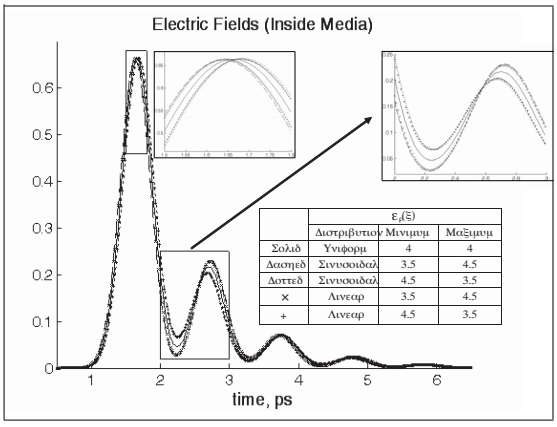

Figure 2. Electric fields inside various dielectric slabs (incident pulse width = 0.2084 ps).

media. The reference case uses the slab of constant permittivity and represented by a solid line. In this set of plot, the incident pulse width is 0.2084 ps and slab thickness is 150 μm. From the two inserted close-ups, the primary hops show slabs with increasing ε_r (dotted line and "+" signed) delay the electromagnetic fields while decreasing ε_r slabs (dashed line and "×" signed) advance the fields with respect to the constant permittivity case. Reverse behavior is observed in the second hop where the electromagnetic fields experience exactly opposite distribution of permittivity since they were reflected from the right interface of the slab. Figure 3 demonstrates all four sets of electric fields inside media where fields behave alike in different time scales despite the two extreme cases are differed by more than 3300 times in pulse width and slab thickness. Figures 3(a) through 3(d) are respectively for four different combinations of incident pulse width and slab thickness.

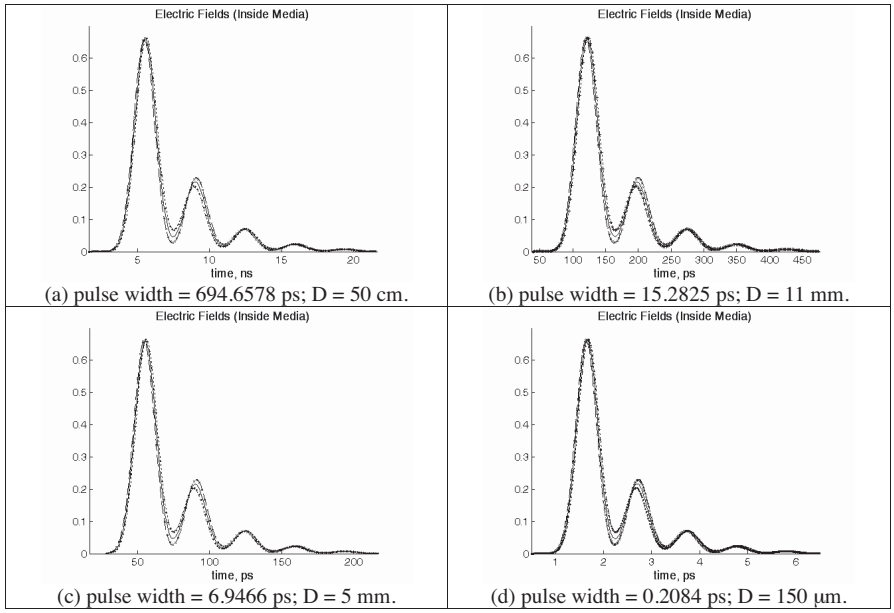

(a) pulse width = 694.6578 ps; D = 50 cm.
(b) pulse width = 15.2825 ps; D = 11 mm.
(c) pulse width = 6.9466 ps; D = 5 mm.
(d) pulse width = 0.2084 ps; D = 150 μm.

Figure 3. Electric fields inside various dielectric slabs.

It is then reasonable to expect they bear identical spectra. In fact, they are. Figures 4 and 5 illustrate the corresponding spectra and phase differences of two different pulse widths of 15.2825 ps and 6.9466 ps. Figure 4 includes the spectrum of total reflection as a reference and Figure 5 gives the phase differences based on the slab with uniform permittivity. It is noted that slabs with permittivity

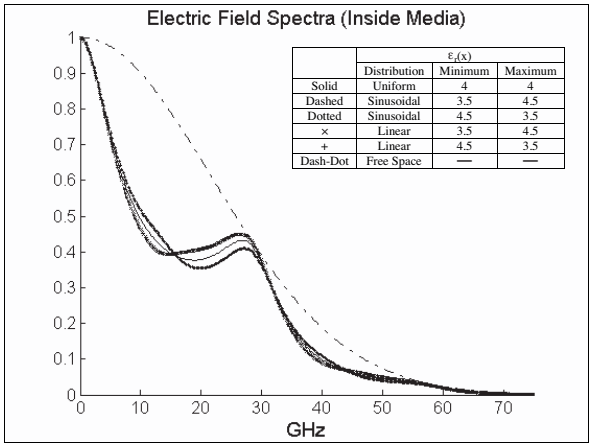

Figure 4. Spectra of various electric fields inside various slabs (incident pulse width = 6.9466 ps).

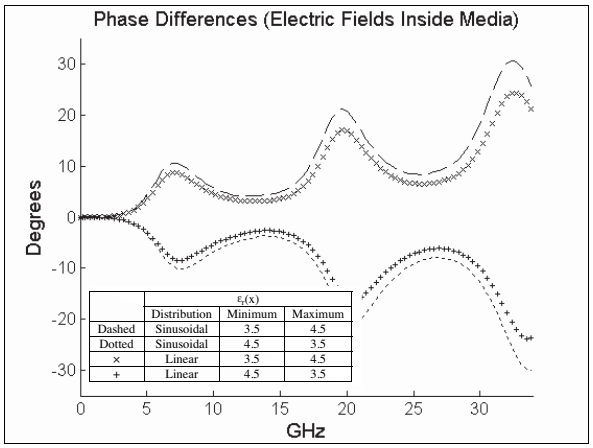

Figure 5. Phase differences of electric fields inside various slabs (incident pulse width = 15.2825 ps).

distributed in sinusoidal form causes more phase change than the linear ones.

The transmitted fields are also recorded and plotted in Figure 6 where the incident pulse width is 694.6578 ps. As expected, transmitted fields emerging from different slabs are compatible. The phase differences for four sets of the transmitted fields were illustrated

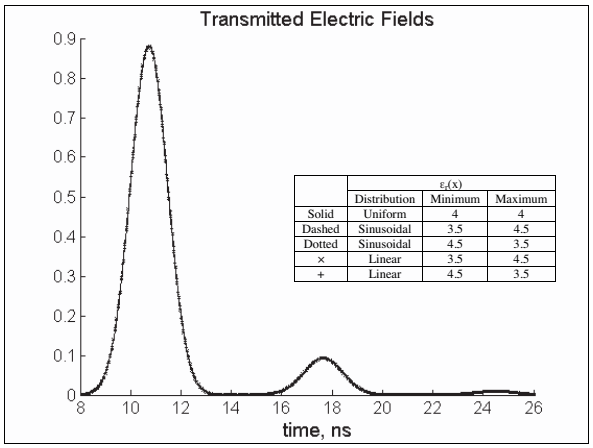

Figure 6. Transmitted electric fields (incident pulse width = 694.6578 ps).

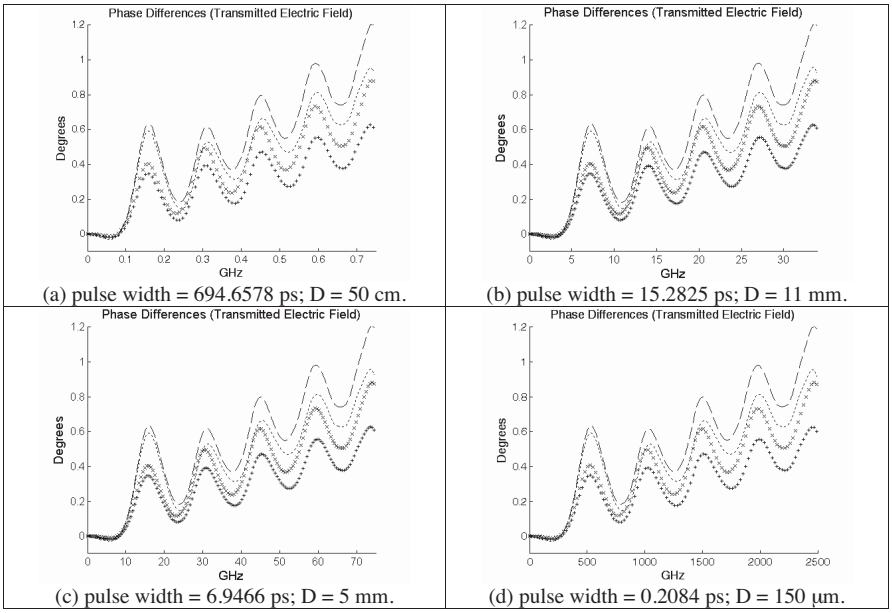

(a) pulse width = 694.6578 ps; D = 50 cm.

(b) pulse width = 15.2825 ps; D = 11 mm.

(c) pulse width = 6.9466 ps; D = 5 mm.

(d) pulse width = 0.2084 ps; D = 150 μm.

Figure 7. Phase differences of transmitted electric fields.

in Figure 7. It is found that the slab with permittivity increasing in sinusoidal form causes more phase change than the others.

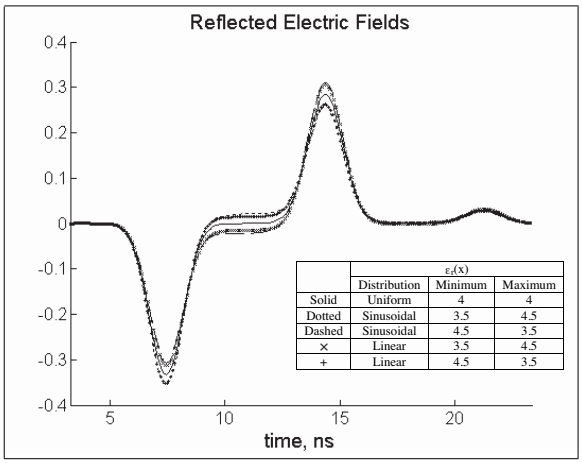

Figure 8. Reflected electric fields (incident pulse width = 694.6578 ps).

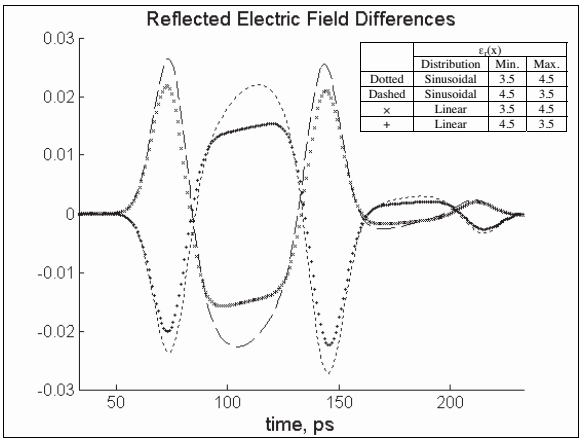

Figure 9. Reflected electric field differences (incident pulse width = 15.2825 ps).

The computational reflected fields are exhibited in Figure 8 giving the following remarks. Despite of the fact that fields were reflected from either air-medium or medium-air interfaces, various reflected fields propagate at identical speed yet with different strengths. The primary reflected fields are stronger in magnitude if slabs have decreasing permittivity while weaker if increasing. Reverse phenomena are observed for the secondary which are reflected from the right interface.

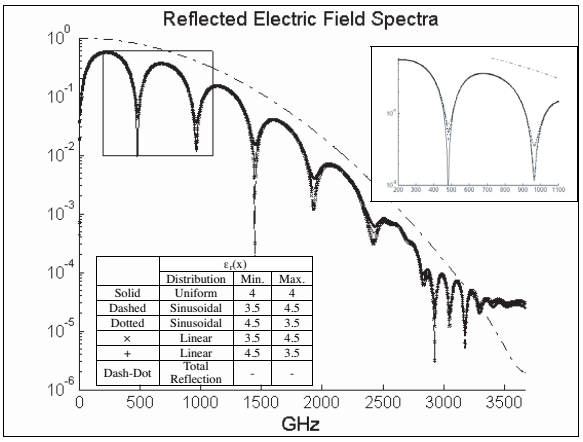

Figure 10. Reflected electric field spectra (incident pulse width = 0.2084 ps).

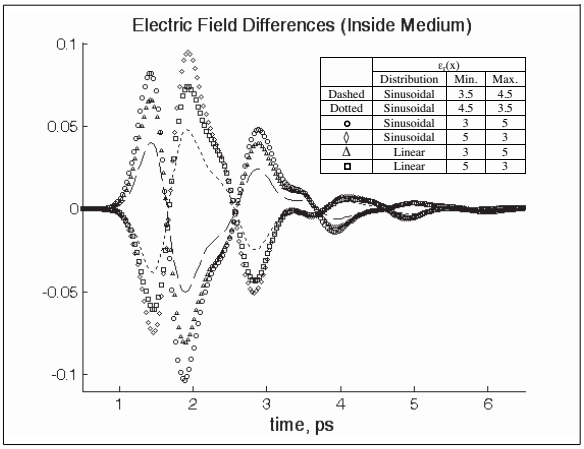

Figure 11. Effects of permittivity deviation on the electric fields inside media (incident pulse width = 0.2084 ps).

Given in Figure 9 are the deviations of the reflected electric fields from the reference with the biggest discrepancy less than 0.03 in magnitude. The spectra of the reflected electric fields were shown in Figure 10 where the incident pulse width is 0.2084 ps. Note that the spectrum of total reflection is included as a reference. The inserted close-up confirms that the reflections from various dielectric slabs bear identical maxima and minima.

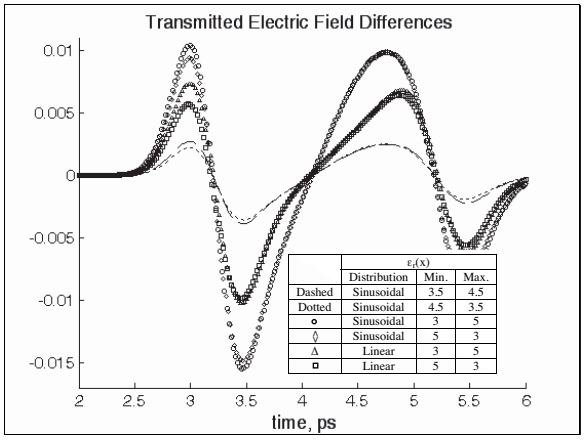

Figure 12. Effects of permittivity deviation on the transmitted electric fields (incident pulse width = 0.2084 ps).

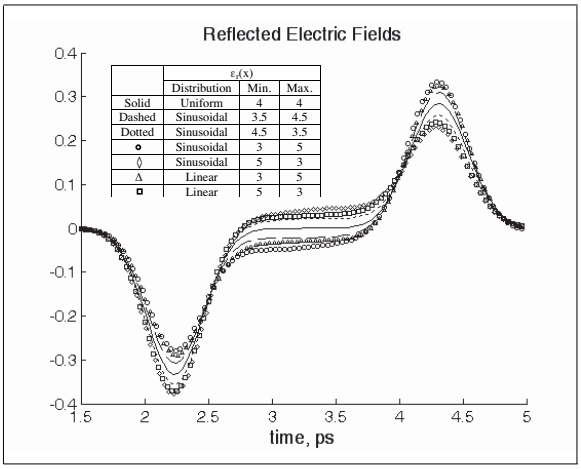

Figure 13. Effects of permittivity deviation on the reflected electric fields (incident pulse width = 0.2084 ps).

The effects of different maximum permittivity deviation (Δ) values on the fields were observed. It is shown that even the maximum permittivity deviation was doubled the transient fields and corresponding spectra reveal indistinguishable trend but with greater distortions which are illustrated in Figures 11, 12, and 13. Once again, since every set of slab displays the same trend in spite of different settings, these three plots are taken from the case with incident pulse

width = 0.2084 ps.

Finally, it is demonstrated earlier the possibility of duplicating identical field propagation characteristics by carefully selecting Gaussian pulse width and dielectric slab thickness. For an incident electromagnetic pulse with a cutoff level of 100 dB and the highest frequency content in spectrum being $f_{\max}$ (in GHz), to duplicate the whole propagation phenomena in different time and frequency ranges, one selects the slab thickness D (in mm) by the following relation: the product of D and $f_{\max}$ is a constant. In the present study we have (D, $f_{\max}$) are (500, 1.0994), (11, 49.9728), (5, 109.9400), (0.150, 3664.8069), respectively, and therefore D multiplies $f_{\max}$ equals 549.702.

5. CONCLUSION

In this paper it has been shown that the characteristic-based method successfully simulates the field propagation through dielectric slabs with varying permittivity in different forms. The numerical results reveal reasonable trends and the effects of non-uniform permittivity on the transmitted and reflected fields, and those inside the dielectric slabs. The corresponding spectra are computed and plotted for close comparisons. By carefully matching the highest frequency content $f_{\max}$ (in GHz) of the incident pulse and the slab thickness D (in mm), one can always duplicate the field propagation pattern in different time scales and frequency ranges. That the product of $f_{\max}$ and D must remain the same value is the rule to follow. It is planned in future to develop the existing numerical procedure for problems in multiple dimensions, or photonic crystal-like structure made of materials with varying permittivity.

ACKNOWLEDGMENT

The authors are grateful to Mr. Michael F. Chen of Cartell Chemical Co., Ltd., Chia-Yi, Taiwan, for making this work possible through the industry-academy cooperation project WFC-E-A1-9511-09.

REFERENCES

1. Shelby, R. A., D. R. Smith, and S. Schultz, "Experimental verification of a negative index of refraction," *Science*, Vol. 292, No. 5514, 77–79, 2001.

2. Pendry, J. B., A. J. Holden, D. J. Robbins, and W. J. Stewart, "Magnetism from conductors and enhanced nonlinear phenomena," *IEEE Trans. Microwave Theory Tech.*, Vol. 47, 2075–2081, Nov. 1999.
3. Pendry, J. B., A. J. Holden, D. J. Robbins, and W. J. Stewart, "Low-frequency plasmons in thin wire structures," *J. Phys. Condensed Matter*, Vol. 10, 4785–4809, 1998.
4. Smith, D. R., W. J. Padilla, D. C. Vier, S. C. Nemat-Nasser, and S. Schultz, "Composite medium with simultaneously negative permeability and permittivity," *Phys. Rev. Lett.*, Vol. 84, No. 18, 4184–4187, 2000.
5. Shelby, R. A., D. R. Smith, S. C. Nemat-Nasser, and S. Schultz, "Microwave transmission through a two-dimensional, isotropic, left-handed metamaterial," *Appl. Phys. Lett.*, Vol. 78, No. 4, 489–491, 2001.
6. Li, Y.-L., "The permittivity based on electromagnetic wave attenuation for rain medium and its applications," *Journal of Electromagnetic Waves and Applications*, Vol. 20, No. 15, 2231–2238, 2006.
7. Gong, S.-H. and J.-Y. Huang, "Accurate analytical model of equivalent dielectric constant for rain medium," *Journal of Electromagnetic Waves and Applications*, Vol. 20, No. 13, 1775–1783, 2006.
8. Yang, R., Y.-J. Xie, P. Wang, and L. Li, "Microstrip antennas with left-handed materials substrates," *Journal of Electromagnetic Waves and Applications*, Vol. 20, No. 9, 1221–1233, 2006.
9. Grzegorczyk, T. M. and J. A. Kong, "Review of left-handed metamaterials: Evolution from theoretical and numerical studies to potential applications," *Journal of Electromagnetic Waves and Applications*, Vol. 20, No. 14, 2053–2064, 2006.
10. Yang, R., Y.-J. Xie, P. Wang, and T. Yang, "Conjugate left- and right-handed material bilayered substrates qualify the subwavelength cavity resonator microstrip antennas as sensors," *Journal of Electromagnetic Waves and Applications*, Vol. 20, No. 15, 2113–2122, 2006.
11. Chen, H., B.-I. Wu, and J. A. Kong, "Review of electromagnetic theory in review of left-handed materials," *Journal of Electromagnetic Waves and Applications*, Vol. 20, No. 15, 2137–2151, 2006.
12. Li, Z. and T. J. Cui, "Novel waveguide directional couplers using left-handed materials," *Journal of Electromagnetic Waves and Applications*, Vol. 21, No. 8, 1053–1062, 2007.

13. Lu, J., B.-I. Wu, J. A. Kong, and M. Chen, "Guided modes with a linearly varying transverse field inside a left-handed dielectric slab," *Journal of Electromagnetic Waves and Applications*, Vol. 20, No. 5, 689–697, 2006.
14. Whitfield, D. L. and J. M. Janus, "Three-dimensional unsteady Euler equations solution using flux splitting," *American Institute of Aeronautics and Astronautics (AIAA) Paper*, 84–1552, 1984.
15. Shang, J. S., "A characteristic-based algorithm for solving 3-d time-domain Maxwell equations," *Electromagnetics*, Vol. 10, 127, 1990.
16. Donohoe, J. P., J. H. Beggs, and M. Ho, "Comparison of finite-difference time-domain results for scattered EM fields: Yee algorithm vs. a characteristic based algorithm," *27th IEEE Southeastern Symposium on System Theory*, March 1995.
17. Ho, M., "Scattering of EM waves from traveling and/or vibrating perfect surface: Numerical simulation," *IEEE Transactions on Antennas and Propagation*, Vol. 54, No. 1, 152–156, January 2006.
18. Ho, M., "Scattering of eelectromagnetic waves from vibrating perfect surfaces: Simulation using relativistic boundary conditions," *Journal of Electromagnetic Waves and Applications*, Vol. 20, No. 4, 425–433, 2006.
19. Ho, M. and F.-S. Lai, "Effects of medium conductivity on eelectromagnetic pulse propagation onto dielectric half space: One-dimensional simulation using characteristic-based method," *Journal of Electromagnetic Waves and Applications*, Vol. 21, No. 13, 1773–1785, 2007.
20. Ho, M., "Propagation of electromagnetic pulse onto a moving lossless dielectric half-space: One-dimensional simulation using characteristic-based method," *Journal of Electromagnetic Waves and Applications*, Vol. 19, No. 4, 469–478, 2005.